Series and Parallel Resonance Problem of Wideband Frequency Harmonic and Its Elimination Strategy

Zhikang Shuai, *Member, IEEE*, Dingguo Liu, John Shen, *Fellow, IEEE*, Chunming Tu, Ying Cheng, and An Luo, *Senior Member, IEEE*

***Abstract*—The extensive use of pulse width modulation control technology in smart grid will lead to prominent enlargement of high-frequency harmonics. The effects of the distributed capacitances of transmission line and transformer that are neglected previously will be very obvious. The performance of the traditional harmonic eliminating method for wideband harmonic is limited, which will lead to huge challenge to the analysis, evaluation, and elimination of harmonics as well as series and parallel resonance problem. In this paper, to accurately describe the influence of wideband harmonic on smart grid, the multiterminal analysis model of harmonic degradation in smart grid is established, especially the distributed capacitances of the transmission line and the transformer are considered. Then, a novel topology of hybrid active power filter (HAPF) for resonance damping and multitype harmonic eliminating is proposed. The resonance damping model of the new topology is established; analysis results indicate that the proposed HAPF has a good harmonic resonance damping characteristic. Both simulation and experimental results have validated the validity of the theoretical analysis in this paper.**

***Index Terms*—Harmonic elimination, power quality, series and parallel resonance, wideband frequency harmonics.**

I. Introduction

With the development of smart grid and the widely use of renewable energy sources, the type and characteristic of the power as well as the topology of the grid have changed obviously [1]–[3]. Therefore, power quality problems are increasingly prominent and present new characteristics. Renewable energy resources (with the characteristic of fluctuation, intermittence, and uncertainty) connect to the grid by power conversion, could lead to the randomness of harmonic problems. More and more power electronic equipment applying to renewable energy generations and flexible control technologies are based on the pulse width modulation (PWM) control technology; and converters generally based on transistors are also gradually developed into PWM technologies, so in the smart grid, the mid-order and high-order frequency harmonic will greatly increase [4], [5]. The applying of voltage-type harmonic source such as high-frequency switch power sources will cause voltage-type harmonic problems, significantly leading to interaction coupled of different harmonic sources. It is hard for traditional power filters to suppress current-type harmonics over 1 kHz effectively, so harmonics in the grid will appear wideband characteristics, and also voltage-type harmonics significantly increase. The distributed capacitance of transmission lines, which has been neglected previously, will affect the harmonic problems significantly. Wideband frequency and multitype interaction couple harmonics will bring a new challenge to the operations of the grid.

People have begun to explore characteristics of power quality problems in the smart grid, for example, the detection and classification of power quality adapting to digital technology [6], [7], power quality in distribution network [8], [9], the stability problem of multiterminal HVDC system [10], [11], the evaluation index and liability evaluation method of power quality [12], [13], power quality standards of the dc transmission technology, and the economic method of power quality. However, most of the studies always focused on harmonic problems of particular distributed microsource, such as the mechanism analysis and elimination method of power quality problems caused by wind power, photovoltaic power generation, or electric vehicles. Some literature works discussed the power quality problems of the microgrid and the distribution system containing the microgrid [14]–[16]. These literature works point out that there are many unique issues related to the power quality in the microgrid and distribution system containing the microgrid. The power quality problems, such as voltage fluctuations, flickers, and the frequency, which are brought by wind farm are proposed in [16] and [17]. A stable microgrid system, which uses hybrid systems containing micro turbines, fuel cell, and others to deal with frequency fluctuations, is presented in [18] and [19]. The work in [20] indicates that there is an interaction coupling among a large number of microsource inverters, so it is a big challenge to adjust their power quality.

In this paper, wideband frequency harmonic problems in the smart grid are discussed. In Section II, based on the analysis of the influence of the distributed capacitance, the mechanism model of series and parallel resonance problem of wideband frequency harmonic is established, and then, the resonance mechanisms of different types of harmonic sources are studied. In

Manuscript received December 3, 2012; revised February 24, 2013; accepted May 10, 2013. Date of current version October 15, 2013. This work was supported by the National Natural Science Foundation of China under Project 51207048, the New Teacher Fund for Doctor Station, the Ministry of Education under Grant 20120161120011, and the Plan for the Growth of Young Teachers, Hunan University. Recommended for publication by Associate Editor A. Muetze.

Z. Shuai, D. Liu, C. Tu, and A. Luo are with the College of Electrical and Information Engineering, Hunan University, Changsha 410082, China (e-mail: zhikangshuai@hotmail.com; dingguoliu@163.com; chunming_tu@263.net; an_luo@126.com).

J. Shen is with the Department of Electrical and Computer Engineering, University of Central Florida, Orlando, FL 32816 USA (e-mail: zjohnshen@gmail.com).

Y. Cheng is with Hunan Electric Power Corporation, Changsha 410082, China (e-mail: ying517@163.com).

Digital Object Identifier 10.1109/TPEL.2013.2264840

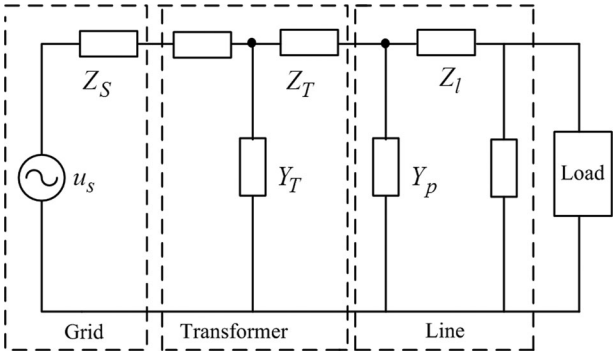

Fig. 1. Single-phase equivalent circuit of the grid.

Section III, a novel topology of hybrid active power filter (HAPF) for wideband and multitype harmonic eliminating is proposed, and its principle and resonance damping characteristics are analyzed in detail. In Section IV, a control method based on the fundamental magnetic flux compensation theory is described. Simulation and experimental results have verified that the novel HAPF has a good performance in harmonic resonance suppression.

II. Series and Parallel Resonance Problem of Wideband Frequency Harmonic

A. Equivalent Circuit of the Smart Grid

To establish the analysis model of harmonic degradation in the grid, equivalent circuit of the grid is discussed first. Especially, the parameters such as the distributed capacitances of transmission line and transformer that are neglected previously will be considered carefully. The lumped-parameter π-type equivalent circuit of the transmission line is difficult to describe its characteristics when the frequency of harmonics and length of the line vary, so distributed-parameter equivalent circuit of the transmission line is adopted in this paper. For a distribution transformer, winding parameters Z_T and excitation parameters Y_T are the main parameters that mainly influence its characteristics, while for a high-frequency transformer, distributed capacitances should be considered [21]. In the smart grid, the frequency of the character harmonic is generally less than 1 kHz, which is far less than the working frequency of high-frequency transformer. So in this paper, the influence of the distributed capacitances is not considered. The single-phase equivalent circuit of the grid is shown in Fig. 1, where u_s is the supply voltage, Z_s is the equivalent impedance of the grid, Z_T and Y_T are the equivalent impedance of the transformer, and Z_l and Y_p are the equivalent impedances of the transmission line.

Fig. 2 shows the mode of the transmission line based on the equivalent π-type model.

From Fig. 2(a), the series and parallel components of the equivalent π model of the long-distance transmission can also be obtained (the calculation process is in the Appendix)

$$\begin{cases} Z_l(h) = Z_C(h)\mathrm{sh}(\gamma(h)l) \\ Y_P(h) = \frac{\mathrm{ch}(\gamma(h)l)-1}{Z_C(h)\mathrm{sh}(\gamma(h)l)} \end{cases}. \tag{1}$$

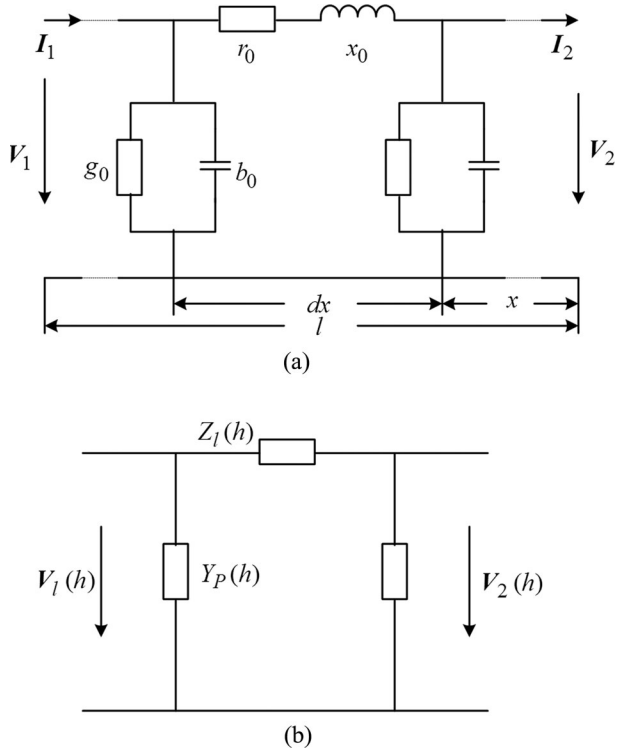

Fig. 2. Model of transmission line based on the equivalent π-type model. (a) Distributed-parameter equivalent circuit of the transmission line in harmonic domain. (b) Lumped-parameter equivalent circuit of the transmission line in harmonic domain.

So the accurate model of lumped-parameter π-type equivalent circuit of the long-distance transmission line can be shown in Fig. 2(b). The equivalent impedance of the line is

$$Z(h) = \frac{Z_l(h)Y_P(h)+1}{Y_P(h)[Z_l(h)Y_P(h)+2]}. \tag{2}$$

Simulations of (2) have been carried out with MATLAB software. The X-axis is the order of the harmonics, the Y-axis is the length of the transmission line, and the Z-axis is the amplitude of the equivalent impedance.

From Fig. 3, it can be seen that when the distributed capacitance is considered, the equivalent impedances of long-distance transmission line change evidently. There is a maximal value in the part of low frequency as the short length; this is because when the line length is very short, the equivalent impedance is mainly determined by the distributed capacitance. However, the transmission line of the grid could not be too short, so the maximal value does not appear in operation. Moreover, there are three significant impedance bands with the variation of frequency and line length. So different types of harmonics certainly lead to the fluctuations of harmonic current and harmonic voltage during transferring in long lines, and the series or parallel resonance problem may occur. The accurate model of lumped-parameter equivalent circuit of the long-distance transmission line established in this paper reflects the characteristics of the distribution line, and also reasonably manifests the impedance and admittance characteristics when containing harmonic currents in transmission lines. So, the model is adopted to study

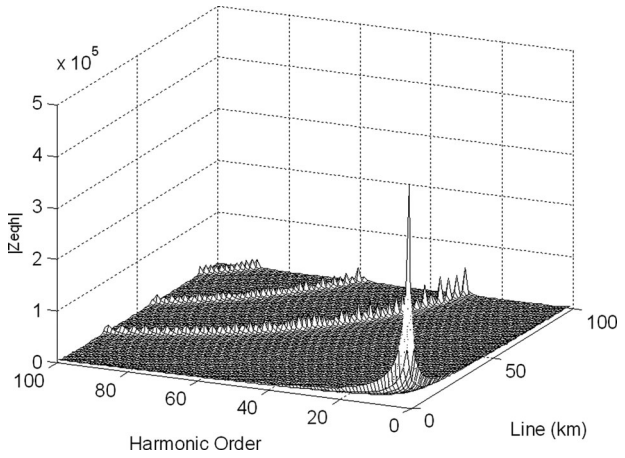

Fig. 3. Variation of the equivalent impedances of long-distance transmission line with changes of harmonic orders and line length.

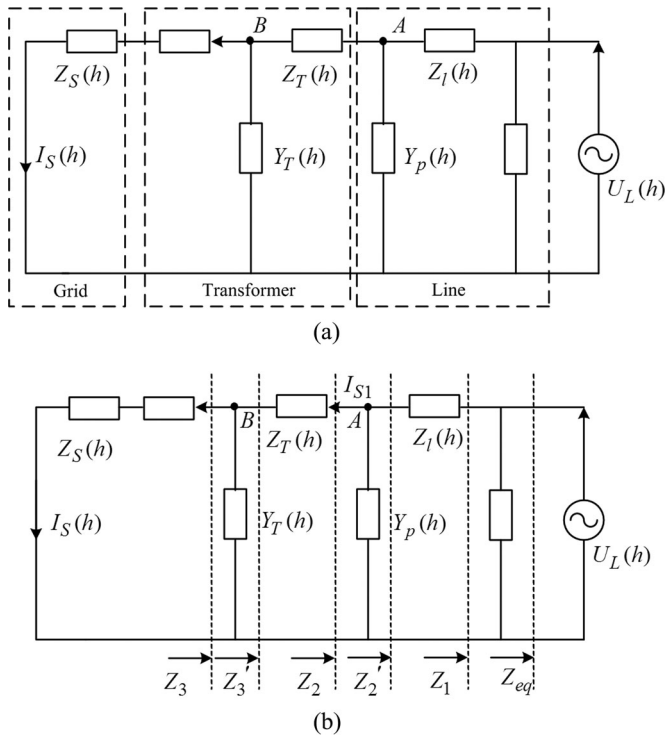

Fig. 4. Analysis model of resonant mechanism when voltage-type harmonic is considered. (a) Electrical model of the grid when voltage-type harmonic is considered. (b) Impedance network when voltage-type harmonic is considered.

the series and parallel resonance problems caused by wideband frequency harmonics.

B. Resonant Mechanism Caused By Voltage-Type Harmonic

With the development of the smart grid, the voltage-type harmonic source has taken more and more important roles, and frequency ranges of harmonics also gradually increase. Fig. 4 shows the analysis model of resonant mechanism when voltage-type harmonic is considered, where $Z_S(h)$ is the equivalent impedance of the grid, $Z_{T1}(h)$ is the impedance in the primary side of the transformer, $Z_m(h)$ is the equivalent impedance of the transformer, $Z_{T2}(h)$ is the impedance in the secondary side of the transformer, and "//" represents parallel computing.

From Fig. 4(b), it can be seen that

$$\begin{cases} Z_3(h) = Z_S(h) + Z_{T1}(h) \\ Z_3'(h) = Z_3(h)//Z_m(h) \\ Z_2(h) = Z_3'(h) + Z_{T2}(h) \\ Z_2'(h) = Z_2(h)//Y_p(h) \\ Z_1(h) = Z_2'(h) + Z_l(h) \\ Z_{\rm eq}(h) = Z_1(h)//Y_p(h). \end{cases} \tag{3}$$

According to (3), we can get that

$$\frac{I_S(h)}{U_L(h)} = \frac{Z_m(h)}{Z_{\rm eq}(h)[Z_1(h)Y_p(h)+1][Z_2(h)Y_p(h)+1][Z_m(h)+Z_3(h)]} \tag{4}$$

$$\frac{U_B(h)}{U_L(h)} = \frac{Z_S(h)\times Z_m(h)}{Z_{\rm eq}(h)\times[Z_1(h)Y_p(h)+1][Z_2(h)Y_p(h)+1][Z_m(h)+Z_3(h)]} \tag{5}$$

$$\frac{U_A(h)}{U_L(h)} = \frac{Z_2(h)}{Z_{\rm eq}(h)\times[Z_2(h)Y_p(h)+1]}. \tag{6}$$

Equations (4)–(6) are the supply harmonic current caused by voltage-type harmonic source, harmonic voltage amplification of the primary and secondary sides of the transformer, respectively. Simulations, as shown in Fig. 4, of (4)–(6) have been carried out with MATLAB software.

Fig. 5 shows that the ratio of the supply harmonic current caused by the voltage-type harmonic to the voltage-type harmonic source is less than 10^{-4}. That is, the supply harmonic current caused by voltage-type harmonic is very small. From Fig. 5(b) and (c), we can see that there is little difference between amplifications in the primary and the secondary side of the transformer. In other words, the harmonic amplification of the voltage-type harmonic source is mainly caused by the distributed capacitance and equivalent impedance of the long-distance transmission lines.

C. Resonant Mechanism Caused By Current-Type Harmonic

Fig. 6 shows the resonant mechanism analysis model of current-type harmonic source. Parameters are the same with those in Fig. 4.

From Fig. 6, we can see that

$$\frac{I_S(h)}{I_L(h)} = \frac{Z_m(h)}{[Z_1(h)Y_p(h)+1][Z_2(h)Y_p(h)+1][Z_m(h)+Z_3(h)]} \tag{7}$$

$$\frac{I_{S1}(h)}{I_L(h)} = \frac{1}{[Z_1(h)Y_p(h)+1][Z_2(h)Y_p(h)+1]}. \tag{8}$$

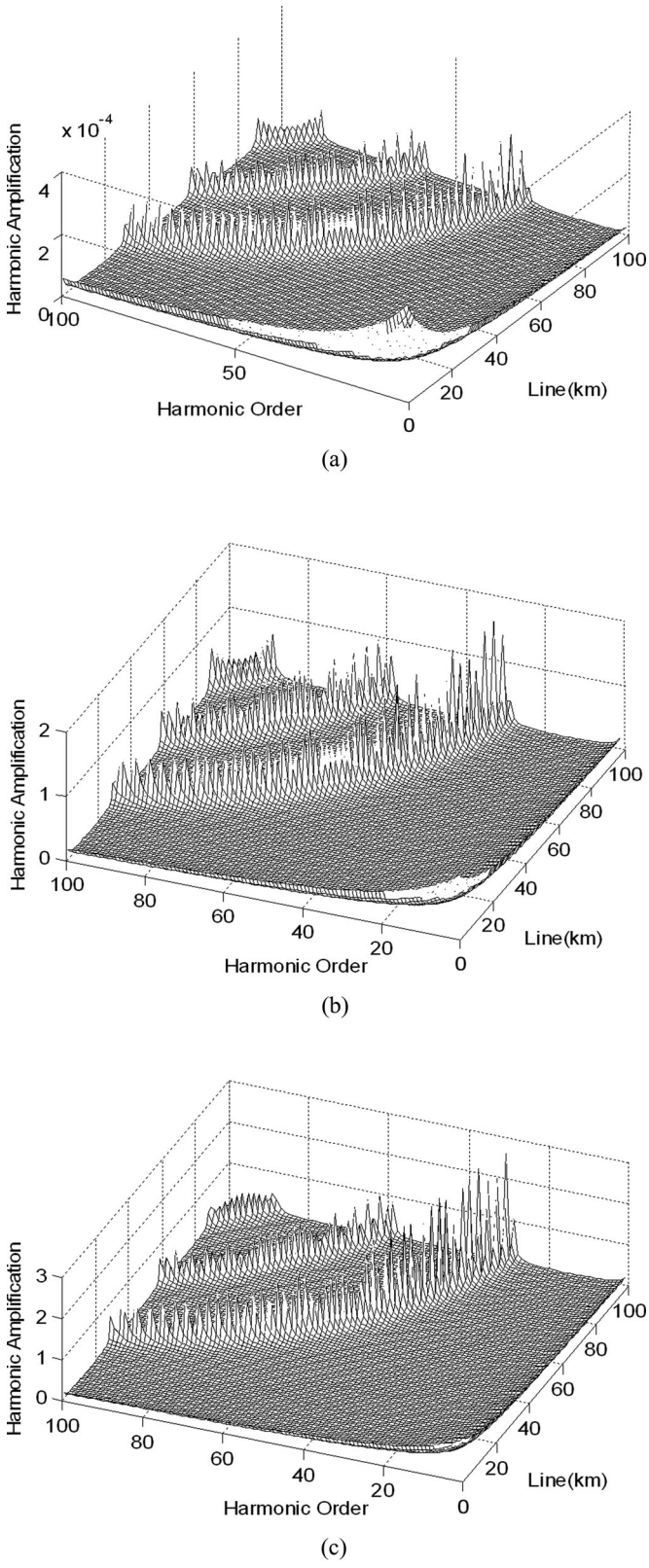

Fig. 5. Simulation diagram of harmonic resonance when voltage-type harmonic is considered. (a) Harmonic current caused by voltage-type harmonic. (b) Harmonic voltage amplifications in the primary side of the transformer caused by voltage-type harmonic. (c) Harmonic voltage amplifications in the secondary side of the transformer caused by voltage-type harmonic.

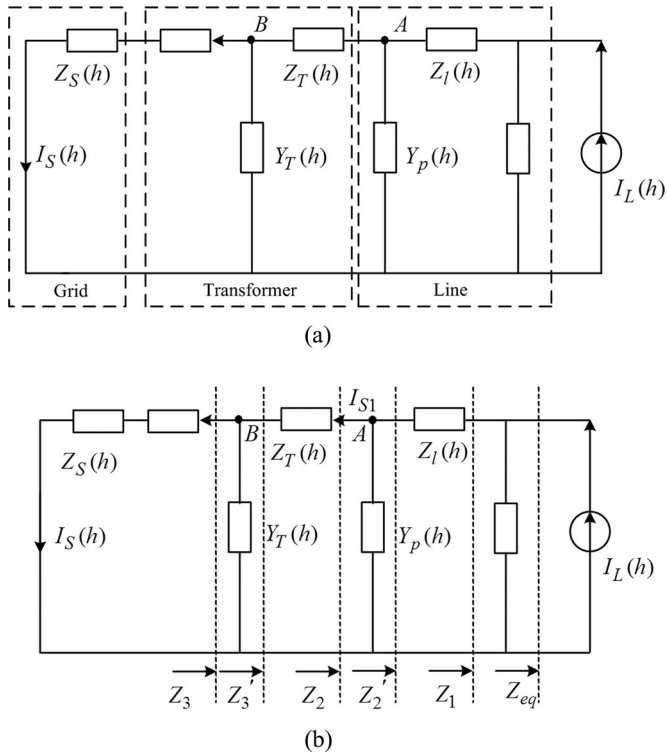

Fig. 6. Analysis model of resonant mechanism when current-type harmonic is considered. (a) Electrical model of the grid when current-type harmonic is considered. (b) Impedance network when current-type harmonic is considered.

Equations (7) and (8) are harmonic current amplifications in the primary and secondary sides of the transformer, respectively. Simulations of (7) and (8) have been carried out with MATLAB software. The results are shown in Fig. 7.

Fig. 7 shows that under the influence of the equivalent impedance and distributed capacitance of the transmission line, the harmonic resonance problem may occur. Especially, with the increasing of frequency or transmission distances, the resonance problems may more serious. According to Fig. 7(a) and (b), there is little difference in amplifications, which is because the leakage reactance of the transformer is far greater than the impedance of transformer winding, and there are large amount of harmonic currents passing through between the primary and secondary sides. So the resonance problem is mainly caused by the distributed capacitance and equivalent impedance of the transmission lines.

III. New HAPF for Harmonic Resonance Elimination

The wideband frequency harmonic problem, with high randomicity and multitype interaction, will be an important part of power quality problems in the smart grid. Especially, the harmonic resonance problem caused by distributed capacitances of transmission line and transformer could not be ignored. In this section, a novel topology of HAPF for resonance damping, wideband frequency, and multitype harmonic eliminating is proposed.

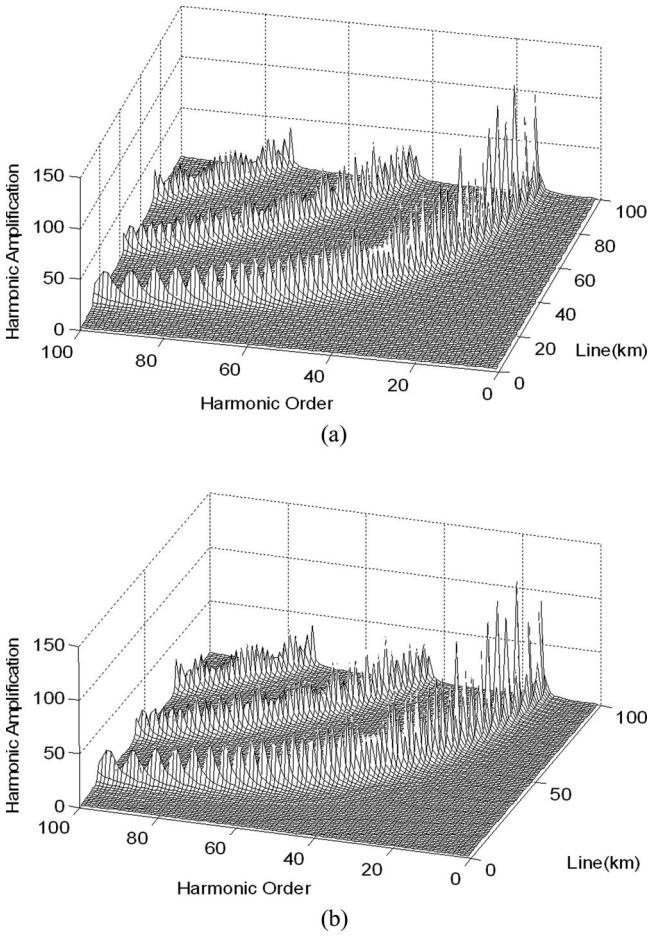

Fig. 7. Simulation diagram of harmonic resonance when current-type harmonic is considered. (a) Harmonic current amplifications in the primary side of the transformer causing by current-type harmonic. (b) Harmonic current amplifications of the secondary side of the transformer causing by current-type harmonic source.

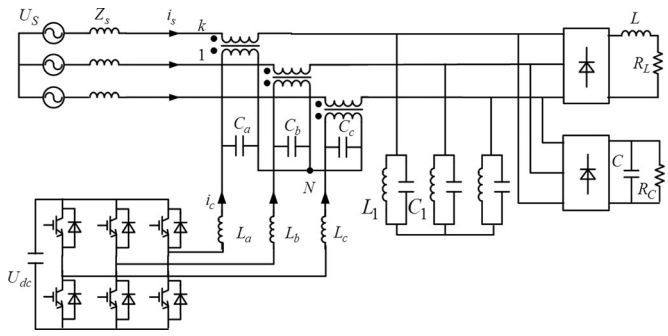

Fig. 8. Topology of the novel HAPF for wideband frequency and multitype harmonic eliminating.

A. Topology of the Novel HAPF for Wideband Frequency and Multitype Harmonic Eliminating

The topology of the proposed HAPF is shown in Fig. 8. The novel topology is mainly composed of a series APF and a parallel PPF. In the series APF, a VSI inverter is connected to the grid through an *LC* filter and a series transformer. It is mainly used for compensating harmonic voltage of nonlinear loads and improving the performance of the passive filter. The parallel PPF is a group of parallel resonant *LC* bandstop filter, which is the turned at fundamental frequency. The PPF is mainly used for eliminating harmonic current and compensating some reactive power when adjusting the resonant frequency.

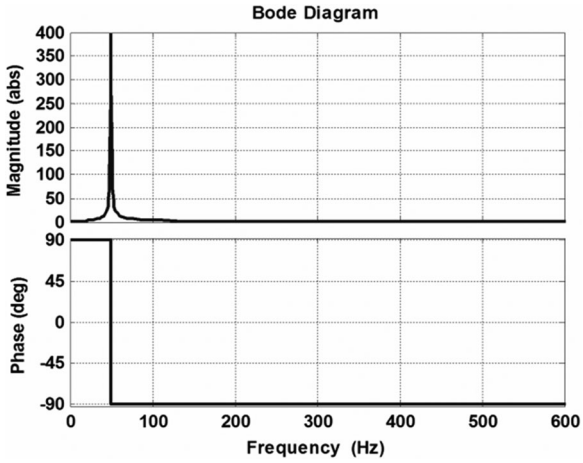

Fig. 9. Amplitude frequency characteristics of the parallel-tuned PPF.

B. Principle of the Novel HAPF

Series-tuned PPF can compensate reactive power and eliminate characteristic harmonic efficiently. However, there will be great harmonic currents in *LC* series-tuned PPF when the grid voltage is distorted or the load contains voltage-type harmonic source. Moreover, the power factor of ac side of the PWM-type inverter is generally high, even close to 1, so it has little need for reactive power compensation. Therefore, the PPF part in the proposed topology adopts a bandstop filter which is connected in parallel and tuned at fundamental frequency. The PPF presents low impedance for high-order harmonics, but does high impedance for low-order harmonics. It also could effectively suppress the low-order harmonic current flowing through the PPF when the grid voltage is distorted or the load contains voltage-type harmonic source. Consequently, it overcomes the disadvantage of the conventional *LC* series-tuned PPF.

The impedance transfer function of parallel-tuned PPF can be expressed as

$$Z_p(s) = \frac{sL_1}{s^2 L_1 C_1 + 1}. \tag{9}$$

Fig. 9 shows the amplitude frequency characteristics of the parallel-tuned PPF. From Fig. 9, it can be seen that the impedance of the PPF on fundamental frequency is large; it is relatively small for the low-frequency harmonics, but for the high-frequency harmonics, the impedance is very small. So it provides current channel for high-frequency harmonics and can avoid vast low-order harmonic current flowing through the passive filter when load-side contains voltage-type harmonic.

In this paper, the APF part in the proposed HAPF is based on the principle of the fundamental magnetic flux compensation

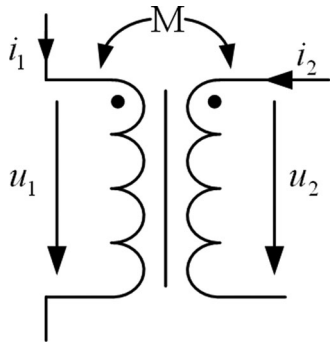

Fig. 10. Series transformer circuit.

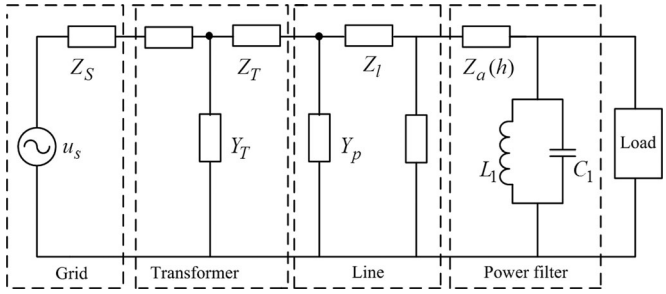

Fig. 11. Single-phase equivalent circuit of the proposed HAPF.

method. The voltage source inverter is controlled to generate a fundamental current in the secondary side of the transformer which could meet the compensation requirement. So the series APF presents low impedance at the fundamental frequency, but the impedance of the grid in harmonic domain increases, which will force the harmonic current flowing into the PPF and improve the performance of PPF. Meanwhile, the series APF produces a compensation voltage whose magnitude is equal and the direction is opposite to the load and grid background harmonic voltage, so the series and parallel resonance can effectively inhibited.

The series transformer in the proposed HAPF can be shown as Fig. 10, assuming the transformer ratio is k and current in the primary side is I_1 (containing the fundamental current and harmonic current); according to fundamental wave magnetic flux compensation theory, if the voltage-type PWM inverter produces a current I_2, if I_2 satisfies (10), the main magnetic flux of the transformer is zero

$$I_{1f} + I_2/k = 0 \tag{10}$$

where I_{1f} and I_2 are the fundamental current in the primary side of the transformer and the total current in the secondary side of the transformer, respectively.

So when the amplitude of the current injected to the secondary winding is k times of the fundamental component in the primary windings, and being the opposite of phase, the fundamental main magnetic flux of the transformer is zero. At this time, the leakage impedance of the primary side for fundamental frequency is very small and assumed as $r_1 + jx_1$, while the impedance for the nth harmonic is n times of that for the fundamental frequency excitation impedance, i.e., jnx_m. Generally, the leakage impedance of the transformer is usually much less than the magnetizing impedance. The ratio of the magnetizing impedance to the leakage impedance exceeds 100 for the fundamental. Therefore, the ratio between transformer impedance to the nth harmonic current and that to fundamental current exceeds $100n$, thus forcing the harmonic current flowing into the PPF, which plays a good role in the harmonic eliminating.

According to the analysis above, the single-phase equivalent circuit of the proposed HAPF can be shown as Fig. 11. For the fundamental frequency, $Z_a^{(1)} = r_1 + jx_1$. For the harmonics, $Z_a^{(n)} \approx jnx_m = j\omega_n L_m$, where ω_n is the harmonic angular frequency and L_m is the magnetizing inductance of the transformer.

C. Impedance Characteristic Analysis of the Proposed HAPF

According to Fig. 11, the transfer function of the equivalent input impedance $Z_{\text{in}}(s)$ and the equivalent output impedance $Z_o(s)$ of the proposed HAPF can be expressed as

$$Z_{\text{in}}(s) = Z_a(s) + Z_p(s) \approx \frac{L_1 C_1 L_m s^3 + (L_m + L_1)s}{L_1 C_1 s^2 + 1} \tag{11}$$

$$Z_o(s) = \frac{1}{\frac{1}{Z_a(s)} + \frac{1}{Z_p(s)}} \approx \frac{L_1 L_m s}{L_1 C_1 L_m s^2 + L_1 + L_m}. \tag{12}$$

The amplitude frequency characteristics of $Z_{\text{in}}(s)$ and $Z_o(s)$ are shown in Fig. 12.

From Fig. 12(a), it can be seen that the equivalent input impedance of the proposed HAPF in harmonic domain is inductive and large. With the increase in frequency, the value of $Z_{\text{in}}(s)$ increases. Moreover, the larger the transformer magnetizing impedance, the larger the value of $Z_{\text{in}}(s)$, so $Z_{\text{in}}(s)$ is mainly depends on the transformer magnetizing impedance. From the frequency response characteristic, we can see that harmonic series resonance phenomenon always does not exist. As the equivalent input impedance is very large, series harmonic resonance caused by the distorted grid voltage can be restrained.

From Fig. 12(b), it can be seen that output impedance value of the proposed HAPF in harmonic domain is capacitive and small. With the increase in frequency, the input impedance decreases; moreover, the variety of the magnetizing impedance has little effect on $Z_o(s)$, so $Z_o(s)$ mainly depends on the PPF. As the value of $Z_o(s)$ is small, the proposed HAPF has a good performance in harmonic eliminating, and the parallel harmonic resonance also can be restrained.

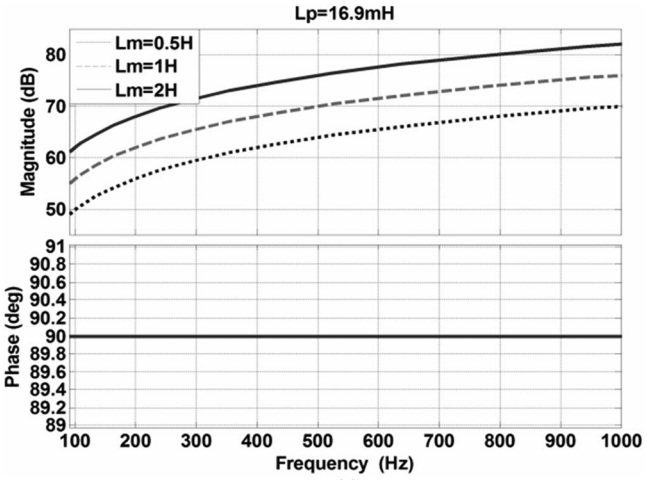

(a)

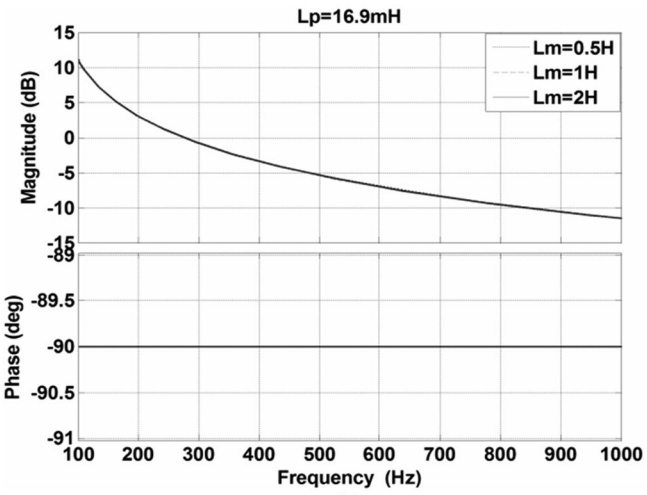

(b)

Fig. 12. Amplitude frequency characteristics of $Z_{\rm in}(s)$and $Z_o(s)$. (a) Amplitude frequency characteristics of $Z_{\rm in}(s)$. (b) Amplitude frequency characteristics of $Z_o(s)$.

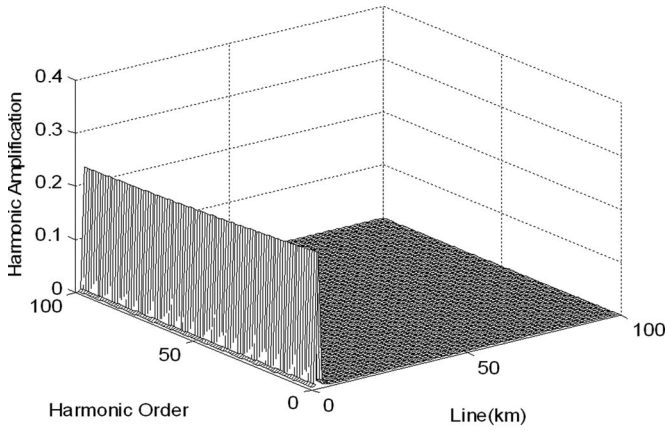

(a)

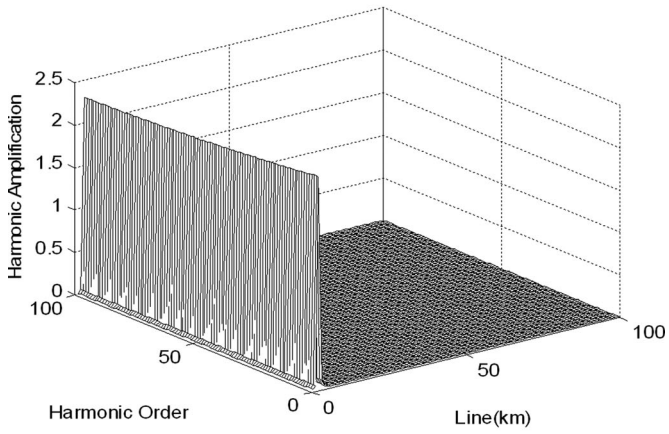

(b)

Fig. 13. Harmonic resonance elimination characteristics for voltage-type harmonic. (a) Ratio of the supply harmonic current to the load harmonic voltage. (b) Ratio of the supply harmonic voltage to the load harmonic voltage.

D. Harmonic Resonance Elimination Characteristics of the Proposed HAPF

From Fig. 11, we can see that

$$\begin{cases} Z_3(h) = Z_S(h) + Z_{T1}(h) \\ Z_3'(h) = Z_3(h)//Z_m(h) \\ Z_2(h) = Z_3'(h) + Z_{T2}(h) \\ Z_2'(h) = Z_2(h)//Y_p(h) \\ Z_1(h) = Z_2'(h) + Z_l(h) \\ \mathrm{Z}_4(h) = Z_1(h)//Y_p(h) \\ Z_4'(h) = \mathrm{Z}_4(h) + Z_a(h) \\ Z_{\rm eq}(h) = Z_4'(h)//Z_p(h). \end{cases} \tag{13}$$

From (13), the ratio of the harmonic current caused by voltage harmonic source to harmonic source when the proposed HAPF is adopted can be represented as

Similarly, the ratio of the supply harmonic voltage to the voltage harmonic source is

Simulations of (14) and (15), shown at the bottom of the next page, have been carried out with software MATLAB. The results are shown in Fig. 13.

From Fig. 13, when the proposed HAPF is adopted, the supply harmonic current and voltage caused by voltage-type harmonic are very small, and there is no resonance in the system with the changes of the length of the transmission and frequency of harmonics. When the transmission distance is short, because of the parallel fundamental resonance branch and distributed capacitance, harmonic magnification may occur, but the transmission line cannot be extremely short. So, the proposed HAPF has a good harmonic damping performance for series resonance caused by voltage-type harmonic.

From Fig. 11, the ratio of the supply harmonic current caused by current harmonic source to load harmonic current when the proposed HAPF is adopted can be represented as

Simulations of (16), shown at the bottom of the next page, have been carried out with software MATLAB. The result is shown in Fig. 14.

From Fig. 14, when the proposed HAPF is adopted, the supply harmonic current caused by load harmonic current is very

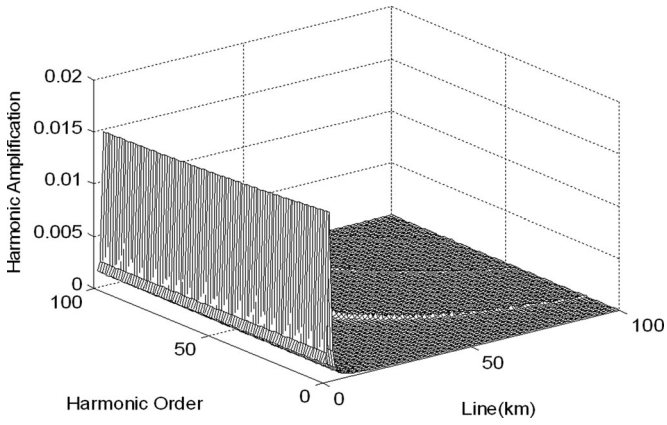

Fig. 14. Harmonic resonance elimination characteristics for current-type harmonic.

small, and there is no resonance with the changes of the length of the transmission and harmonic frequency. So, the proposed HAPF has a good harmonic resonance elimination characteristics caused by current-type harmonic.

IV. Control Method Based on the Fundamental Magnetic Flux Compensation Theory

According to the analysis in Section III-B, the APF part should be controlled to output a fundamental current satisfying fundamental flux compensation condition as shown in (10). Traditional proportional-integral (PI) control is usually adopted to improve the dynamic response and/or to increase the stability margin of a closed-loop system. However, the traditional PI controller may present a poor steady-state error for ac signal. In this paper, a zero steady-state error PI control method based on the transformer fundamental magnetic flux compensation theory is proposed. The proposed control method transforms the error signal of fundamental current into dc signal by coordinate transformation and carries out PI control to dc signal, which can eliminate the system steady-state error. The control block diagram of the proposed control method is shown in Fig. 15.

As shown in Fig. 15, in order to reduce the number of coordinate transformation, the proposed method first detects the supply current i_s(primary current of the series transformer). The secondary current of the transformer can be obtained when i_s is multiplied by the coefficient k. The error of $-ki_s$ and the output current of the inverter i_1 contains the supply harmonic

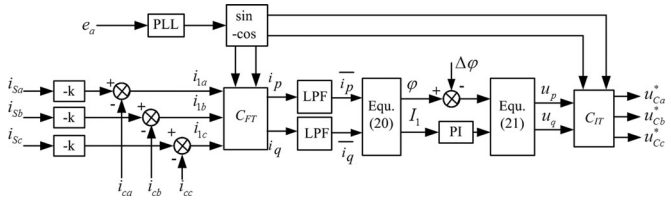

Fig. 15. Control block diagram of the proposed control method.

current and the error of the fundamental reference signal and the compensation signal. From the control block, it can be seen that the proposed control method only carries out PI control to the amplitude of error signal, which can avoid the integral of frequency and phase angle. So the steady-state error can be avoided, and the number of coordinate transformation and the PI controller are also reduced.

In Fig. 15, $\boldsymbol{C_{FT}}$ and $\boldsymbol{C_{IT}}$ are the positive transform matrix and the inverse transform matrix, respectively

$$\boldsymbol{C_{FT}} = \frac{2}{3}\begin{bmatrix} \sin\omega t & \sin(\omega t - 2\pi/3) & \sin(\omega t + 2\pi/3) \\ \cos\omega t & \cos(\omega t - 2\pi/3) & \cos(\omega t + 2\pi/3) \end{bmatrix} \tag{17}$$

$$\boldsymbol{C_{IT}} = \begin{bmatrix} \sin\omega t & \cos\omega t \\ \sin(\omega t - 2\pi/3) & \cos(\omega t - 2\pi/3) \\ \sin(\omega t + 2\pi/3) & \cos(\omega t + 2\pi/3) \end{bmatrix}. \tag{18}$$

Assuming $i_1 = I_1\sin(\omega t + \varphi) + \sum_{n=1}^{\infty} I_n \sin(n\,\omega t + \varphi_n)$, the active current component i_p and reactive current component i_q can be obtained

$$\begin{bmatrix} i_p \\ i_q \end{bmatrix} = \boldsymbol{C_{FT}} \begin{bmatrix} i_{1a} \\ i_{1b} \\ i_{1c} \end{bmatrix}. \tag{19}$$

When the active current component i_p and reactive current component i_q are filtered by a low-pass filter, their dc component can be obtained

$$\begin{cases} \bar{i}_p = I_1\cos\varphi/2 \\ \bar{i}_q = I_1\sin\varphi/2. \end{cases} \tag{20}$$

Equation (20) contains the amplitude and phase information of error signal, and the amplitude and phase information can be

$$\frac{I_S(h)}{U_L(h)} = \frac{Z_{\rm eq}(h)Z_p(h)Z_m(h)}{[\mathrm{Z}_4^{'}(h)+Z_p(h)][Z_1(h)Y_p(h)+1][Z_2(h)Y_p(h)+1][Z_m(h)+Z_3(h)]}. \tag{14}$$

$$\frac{U_B(h)}{U_L(h)} = \frac{Z_3(h)\times Z_{\rm eq}(h)\times Z_p(h)\times Z_m(h)}{[Z_4'(h)+Z_p(h)][Z_1(h)Y_p(h)+1][Z_2(h)Y_p(h)+1][Z_m(h)+Z_3(h)]} \tag{15}$$

$$\frac{I_S(h)}{I_L(h)} = \frac{Z_p(h)Z_m(h)}{[\mathrm{Z}_4^{'}(h)+Z_p(h)][Z_1(h)Y_p(h)+1][Z_2(h)Y_p(h)+1][Z_m(h)+Z_3(h)]}. \tag{16}$$

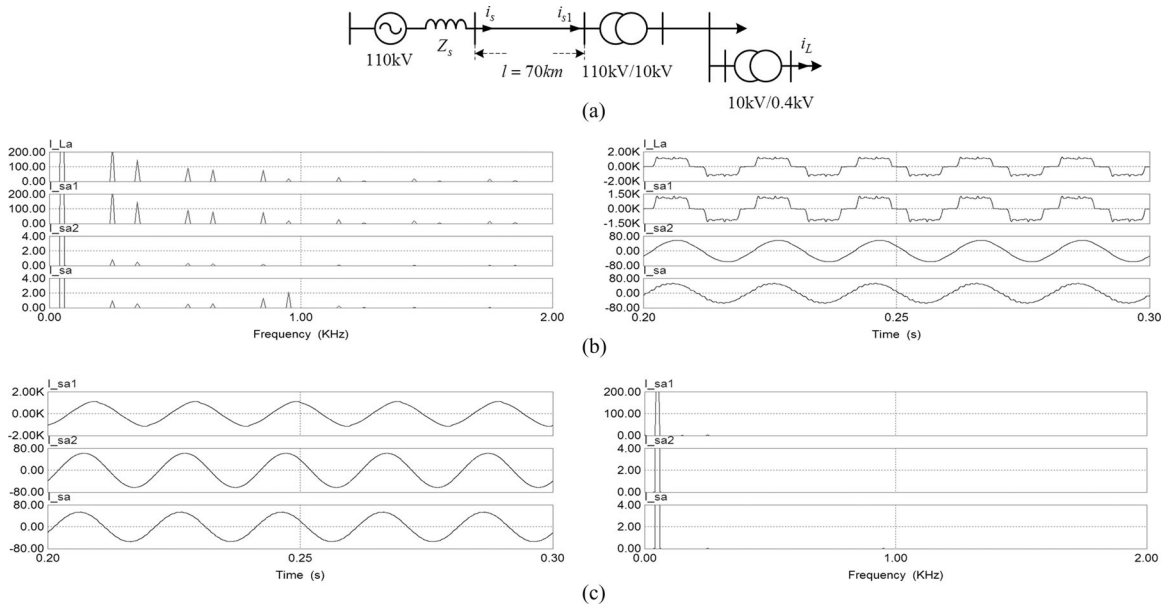

Fig. 16. Simulation results. (a) Main circuit of the simulation system. (b) Current waveforms before the proposed HAPF is adopted. (c) Current waveforms after the proposed HAPF is adopted.

calculated as follows:

$$\begin{cases} I_1 = 2\sqrt{\bar{i}_p^2 + \bar{i}_q^2} \\ \varphi = \arctan(\bar{i}_q/\bar{i}_p). \end{cases} \tag{21}$$

As the amplitude of the error signal is dc value, the goal that output current of the inverter tracking the reference signal without static error can be realized. To improve the compensation performance of the APF, an adjustment angle $\Delta\varphi$ is used to compensate the delay time produced by the detection of the control signal, low-pass filter, etc. Assuming the amplitude and phase angle of fundamental command current signal after PI controller are U_1^* and φ^*, respectively, the instantaneous active component u_p and reactive component u_q of the reference signal can be obtained as

$$\begin{cases} u_p = U_1^* \cos\varphi^*/2 \\ u_q = U_1^* \sin\varphi^*/2. \end{cases} \tag{22}$$

The modulated signal of the inverter can be expressed as

$$\begin{bmatrix} u_{ca}^* \\ u_{cb}^* \\ u_{cc}^* \end{bmatrix} = \mathbf{C_{IT}} \begin{bmatrix} u_p \\ u_q \end{bmatrix}. \tag{23}$$

V. Simulation and Experimental Results

A. Simulation Results

Simulations have been carried out with the software PSIM6.0. The main circuit in the simulations is shown in Fig. 16(a). In Fig. 16(a), the supply voltage is 110 kV, the length of the 110-kV transmission line is 70 km, and the impedance and admittance of per unit length of the line is 0.00113 mH and 0.0044 μF. The equivalent impendence of the 10-kV system is 8 Ω and 20.9 mH; the nonlinear load in the 0.4-kV system is constituted by the inductor filtering three-phase uncontrollable rectifier bridge and capacitor filtering uncontrollable rectifier bridge in parallel, where dc-side inductor of inductor filtering rectifier bridge is 0.3 mH and series resistor 0.5 Ω; the dc-side capacitor of capacitor filtering rectifier bridge is 500 μF and parallel resistor 10 Ω. Other simulation parameters are as follows: the turns ratio of the series transformer is 1:1; the output filter of the inverter $L_a = 3$ mH, $C_a = 20$ μF; the parallel passive filter $L_P = 8.45$ mH, $C_P = 1200$ μF; the dc-side capacitance 10 000 μF. Simulation results are shown in Fig. 16(b) and (c), where $I_{\_sa}$ is the supply current of phase-a in the 110-kV system, $I_{\_sa1}$ is the current of phase-a in the 110-kV system nearing the load, $I_{\_La}$ is the supply current in the 0.4-kV system, and the unit is A_o.

From Fig. 16(b), when the proposed HAPF is not adopted, the supply current in the 0.4-kV system is serious distortion, and the harmonic content in the current spectrum is large; meanwhile, in the 110-kV system, the harmonic resonance problem occurs, especially the 19th harmonic current has increased from 0.028 to 2.13 A, and the amplification is about 76°. From Fig. 16(c), it can be seen that when the proposed HAPF is adopted, supply current in the 0.4-kV system and the 110-kV system are both nearly standard sine waves; the performance of harmonic resonance problem suppression is very significant.

B. Experimental Results

An experimental platform has also been built in the laboratory. In the experiment, the supply voltage is 0.4 kV; the nonlinear load is constituted by the inductor filtering three-phase uncontrollable rectifier bridge and capacitor filtering uncontrollable rectifier bridge, where filtering inductor and its series resistor are, respectively, 30 mH and 30 Ω; filtering capacitor and its parallel resistor capacitor are, respectively, 500 μF and 50 Ω. Series transformer is composed of three single-phase transformers with a turns ratio 1:1. TMS320F2812 digital processor is used to

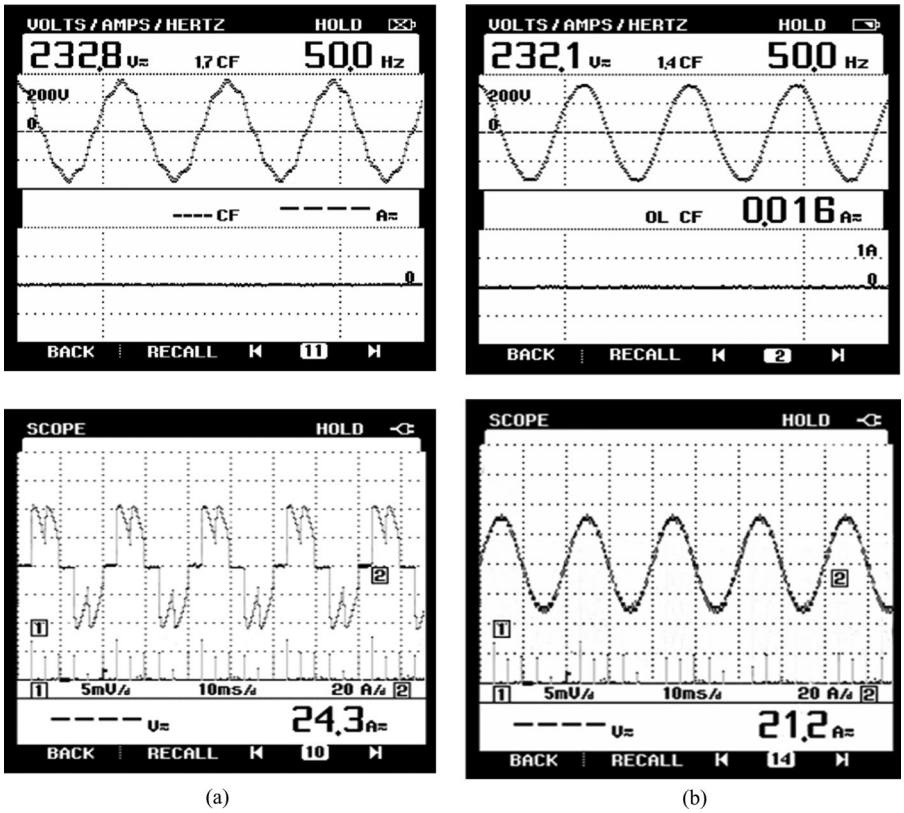

(a) (b)

Fig. 17. Experimental results. (a) Supply voltage and current before the HAPF is adopted. (b) Supply voltage and current after the HAPF is adopted.

play the part of controller, and IGBT module FF150R12ME3G is used as the switching device. Fig. 17 shows the supply voltage and current of phase-A power before and after the proposed HAPF is adopted.

According to Fig. 17, the distortion rate of supply current is 45%, and the distortion rate of supply voltage is 5.3% before the proposed HAPF is adopted, while when the proposed HAPF is put into use, the distortion rate of the supply current reduced to 2.9%, and the distortion rate of supply voltage reduced to 1.28%. So the harmonic contents of supply current and supply voltage are significantly reduced; waveforms of supply current and supply voltage are close to standard sine wave; and the harmonic resonance problem can also be suppressed.

VI. Conclusion

The propagation rule of wideband frequency harmonic in the grid is studied in this paper. Considering the influence of distributed capacitances of the transmission line and the transformer, the multiterminal network analysis model of wideband frequency harmonic deterioration is established, and the mechanism of the series and parallel resonance problems of wideband frequency harmonic in the grid is presented. A novel topology of HAPF for wideband frequency and multitype harmonic eliminating is proposed, and the electrical model of the proposed HAPF is established for the analysis of harmonic resonance suppression caused by different types of harmonics. Simulation and experimental results validated the rationality of the theoretical analysis of the harmonic resonance problem, and also indicated that the proposed HAPF has a good damping performance for different types of harmonics.

Appendix

In this appendix, the calculation of series and parallel components of the equivalent π model of the long-distance transmission is described.

The distributed-parameter equivalent circuit of the long-distance transmission line in harmonic domain is shown in Fig. 2(a). For per unit length of the line, $x = 0$ means the terminal end. The differential equations of the current and voltage are

$$\begin{cases} d\boldsymbol{V} = \boldsymbol{I}(r_0 + j\omega_n L_0)dx \\ d\boldsymbol{I} = (\boldsymbol{V} + d\boldsymbol{V})(g_0 + j\omega_n C_0)dx \end{cases} \tag{24}$$

where ω_n is the angular frequency of the nth harmonic. $z_0 = r_0 + jx_0$ and $y_0 = g_0 + jb_0$ are the impedance and admittance of per unit length of the line, respectively.

From (24), we can see that

$$\frac{d^2\boldsymbol{V}}{dx^2} = (g_0 + j\omega_n C_0)(r_0 + j\omega_n L_0)\,\boldsymbol{V}. \tag{25}$$

From (25), it can be seen that

$$\begin{cases} \boldsymbol{V} = A_1 e^{\gamma x} + A_2 e^{-\gamma x} \\ \boldsymbol{I} = \frac{A_1}{Z_C(h)} e^{\gamma x} + \frac{A_2}{Z_C(h)} e^{-\gamma x} \end{cases} \tag{26}$$

where γ is the propagation constant, and $Z_C(h)$ is the characteristic impedance, and $A_1 = {}^1\!/\!_2(\boldsymbol{V}_2 + Z_C(h)\boldsymbol{I}_2)$, $A_2 = {}^1\!/\!_2(\boldsymbol{V}_2 - Z_C(h)\boldsymbol{I}_2)$. The propagation constant and characteristic impedance are

$$\begin{cases} \gamma(h) = \sqrt{z_0(h)y_0(h)} \approx \omega_n\sqrt{L_0C_0} \\ Z_C(h) = \sqrt{z_0(h)/y_0(h)} \approx \sqrt{\frac{L_0}{C_0}}. \end{cases} \tag{27}$$

Considering the boundary condition $x = 0$, from (26), we can get

$$\begin{cases} \boldsymbol{V}_1 = \boldsymbol{V}_2\ \mathrm{ch}\gamma(h)x + \boldsymbol{I}_2 Z_C(h)\mathrm{sh}\gamma(h)x \\ \boldsymbol{I}_1 = \frac{\boldsymbol{V}_2}{Z_C(h)}\mathrm{sh}\gamma(h)x + \boldsymbol{I}_2\ \mathrm{ch}\gamma(h)x. \end{cases} \tag{28}$$

So, when $x = \mathrm{l}$, it can be seen that

$$\begin{cases} \boldsymbol{V}_1 = \boldsymbol{V}_2\ \mathrm{ch}\gamma(h)l + \boldsymbol{I}_2 Z_C(h)\mathrm{sh}\gamma(h)l \\ \boldsymbol{I}_1 = \frac{\boldsymbol{V}_2}{Z_C(h)}\mathrm{sh}\gamma(h)l + \boldsymbol{I}_2\ \mathrm{ch}\gamma(h)l. \end{cases} \tag{29}$$

Then, from (29), the relationship of voltage and current in the two terminals of the transmission line can be obtained. The series and parallel components of the equivalent π model of the long-distance transmission can also be obtained

$$\begin{cases} Z_l(h) = Z_C(h)\mathrm{sh}(\gamma(h)l) \\ Y_P(h) = \frac{\mathrm{ch}(\gamma(h)l)-1}{Z_C(h)\mathrm{sh}(\gamma(h)l)}. \end{cases} \tag{30}$$

REFERENCES

[1] F. Boico and B. Lehman, "Multiple-input maximum power point tracking algorithm for solar panels with reduced sensing circuitry for portable applications," *Solar Energy*, vol. 86, no. 1, pp. 463–475, Jan. 2012.

[2] R. F. Arritt and R. C. Dugan, "Distribution system analysis and the future smart grid," *IEEE Trans. Ind. Appl.*, vol. 47, no. 6, pp. 2343–2350, Nov. 2011.

[3] T. Wang, F. Fang, X. Wu, and X. Jiang, "Novel filter for stator harmonic currents reduction in six-step converter fed multiphase induction motor drives," *IEEE Trans. Power Electron.*, vol. 28, no. 1, pp. 498–506, Jan. 2013.

[4] L. Yan and B. Lehman, "A capacitor modeling method for integrated magnetic components in DC/DC converters," *IEEE Trans. Power Electron.*, vol. 20, no. 5, pp. 987–996, Sep. 2005.

[5] Z. Shuai, A. Luo, Z. John Shen, W. Zhu, Z. Lv, and C. Wu, "A dynamic hybrid var compensator and a two-level collaborative optimization compensation method," *IEEE Trans. Power Electron.*, vol. 24, no. 9, pp. 2091–2100, Sep. 2009.

[6] Z. Li, P. Wang, H. Zhu, Z. Chu, and Y. Li, "An Improved pulse width modulation method for chopper-cell-based modular multilevel converters," *IEEE Trans. Power Electron.*, vol. 27, no. 8, pp. 3472–3481, Aug. 2012.

[7] U. D. Dwivedi, "Denoising techniques with change-point approach for wavelet-based power-quality monitoring," *IEEE Trans. Power Del.*, vol. 24, no. 3, pp. 1719–1727, Jul. 2009.

[8] N. R. N. Ama, F. O. Martinz, L. Matakas, and F. Kassab, "Phase-locked loop based on selective harmonics elimination for utility applications," *IEEE Trans. Power Electron.*, vol. 28, no. 1, pp. 144–153, Jan. 2013.

[9] A. D. le Roux, H. D. T. Mouton, and H. Akagi, "DFT-based repetitive control of a series active filter integrated with a 12-pulse diode rectifier," *IEEE Trans. Power Electron.*, vol. 24, no. 6, pp. 1515–1521, Jun. 2009.

[10] Y Sun, M. Su, X. Li, H. Wang, and W. Gui, "A General constructive approach to matrix converter stabilization," *IEEE Trans. Power Electron.*, vol. 28, no. 1, pp. 418–431, Jan. 2013.

[11] K Sano and M. Takasaki, "A transformerless D-Statcom based on a multivoltage cascade converter requiring no DC Sources," *IEEE Trans. Power Electron.*, vol. 27, no. 6, pp. 2783–2795, Jun. 2012.

[12] A. Salarvand, B. Mirzeian, and M. Moallem, "Obtaining a quantitative index for power quality evaluation in competitive electricity market," *IET Generation, Transmiss. Distrib.*, vol. 4, no. 7, pp. 810–823, Jul. 2012.

[13] M. Prodanovic and T. C Green, "High-quality power generation through distributed control of a power park microgrid," *IEEE Trans. Ind. Electron.*, vol. 53, no. 5, pp. 1471–1482, Oct. 2006.

[14] A. Khaligh, J. R. Wells, P. L. Chapman, and P. T. Krein, "Dead-time distortion in generalized selective harmonic control," *IEEE Trans. Power Electron.*, vol. 23, no. 3, pp. 1511–1517, May 2009.

[15] Z. Shuai, A. Luo, J. Shen, and X. Wang, "Double closed-loop control method for injection-type hybrid active power filter," *IEEE Trans. Power. Electron.*, vol. 26, no. 9, pp. 2393–2403, Sep. 2011.

[16] M. Azizi, A. Fatemi, M. Mohamadian, and A.Y. Varjani, "Intergrated solution for microgrid power quality assurance," *IEEE Trans. Energy Convers.*, vol. 27, no. 4, pp. 992–1001, Dec. 2012.

[17] L. Sainz, J. J. Mesas, R. Teodorescu, and P. Rodriguez, "Deterministic and stochastic study of wind farm harmonic currents," *IEEE Trans. Energy Convers.*, vol. 25, no. 4, pp. 1071–1080, Dec. 2010.

[18] M. L. S. Rahman, Y Oka, and Shirai, "Hybrid power generation system using offshore-wind turbine and tidal turbine for power fluctuation compensation (HOT-PC)," *IEEE Trans. Sustainable Energy*, vol. 1, no. 2, pp. 92–98, Jul. 2010.

[19] M. Datta, T. Senjyu, A. Yona, T. Funabashi, and K. Chul-Hwan, "A coordinated control method for leveling PV Output power fluctuations of PV–Diesel hybrid systems connected to isolated power utility," *IEEE Trans. Energy Convers.*, vol. 24, no. 1, pp. 153–162, Mar. 2009.

[20] J. H. R. Enslin and P. J. M. Heskes, "Harmonic interaction between a large number of distributed power inverters and distribution network," *IEEE Trans. Power Electron.*, vol. 19, no. 6, pp. 1586–1594, Jun. 2004.

[21] H. Y. Lu, J. G. Zhu, and Y. R. Hui, "Experimental determination of stray capacitances in high frequency transformers," *IEEE Trans. Power Electron.*, vol. 18, no. 5, pp. 1105–1112, Sep. 2003.

Zhikang Shuai (M'11) was born in Shandong, China, on December 19, 1982. He received the B.S. and Ph.D. degrees from the College of Electrical and Information Engineering, Hunan University, Changsha, China, in 2005 and 2011, respectively.

He was with the Hunan University as an Assistant Professor between 2009 and 2012, where he became an Associate Professor at Hunan University in 2012. His research interests include harmonics suppression and reactive power compensation, and active power filters.

Dr. Shuai received the 2010 National Scientific and Technological Awards of China, the 2007 Scientific and Technological Awards from the National Mechanical Industry Association of China.

Dingguo Liu was born in Hunan, China, on June 6, 1979. He received the B.S. and M.S. degrees from the College of Electrical and Information engineering, Hunan University, Changsha, China, in 2005 and 2008, respectively, where he has been working toward the doctoral degree in the College of Electrical and Information Engineering.

His research interests include harmonics suppression, reactive power compensation, and smart grid.

John Shen (M'82–SM'90–F'11) received the B.S.E.E. degree from Tsinghua University, Beijing, China, in 1987, and the M.S. and Ph.D. degrees from Rensselaer Polytechnic Institute, Troy, NY, USA, in 1991 and 1994, respectively, all in electrical engineering.

He is currently an Associate Professor of Electrical Engineering at the University of Central Florida, Orlando, FL, USA. Between 1994 and 1999, he held a variety of positions including Senior Principal Staff Scientist with Motorola Semiconductor Products Sector, Phoenix, AZ, USA. He was with the University of Michigan, Dearborn, as an Assistant and Associate Professor in the Department of Electrical and Computer Engineering between 1999 and 2003. His research interests include power electronics, power semiconductor devices and ICs, power management for computers and telecom equipment, automotive electronics, renewable and alternative energy systems, and electronics manufacturing. He has published more than 80 journal and conference articles, and holds nine issued and several pending U.S. patents in these areas.

Dr. Shen received the 2003 NSF CAREER Award, the 2006 IEEE Transaction Paper Award from the IEEE Society of Power Electronics, the 2003 IEEE Best Automotive Electronics Paper Award from the IEEE Society of Vehicular Technology, and the 1996 Motorola Science and Technology Award. He currently serves as an at-large AdCom member of the IEEE Power Electronics Society and an Associate Editor of the IEEE TRANSACTIONS IN POWER ELECTRONICS.

Chunming Tu was born in Nanchang, Jiangxi, China, on February 16, 1976. He received the M.S. and Ph.D. degrees from Central South University, Changsha, China, in 2001 and 2004, respectively.

He is currently with the College of Electrical and Information engineering, Hunan University, Changsha. His research interests include electric power saving and active power filters.

Ying Cheng was born in Changsha, Hunan, China, on May 17, 1985. She received the B.S. degree from the College of Electrical Engineering, Southwest Jiaotong University, Chengdu, China, in 2007, and the M.S. degree from the College of Electrical and Information engineering, Hunan University, Changsha, in 2010.

She is currently with Hunan Electric Power Corporation, Changsha. Her research interests include power electronics and power quality.

An Luo (SM'10) was born in Chang Sha, China, on July 21, 1957. He received the B.S. and M.S. degrees from Hunan University, Changsha, China, in 1982 and 1986, respectively, and the Ph.D. degree from Zhejiang University, Zhejiang, China, in 1993.

He was with the Central South University, as a Professor between 1996 and 2002. In 2003, he became a Professor at Hunan University. His research interests include power conversion system, harmonics suppression and reactive power compensation, and electric power saving. He has published more than 100 journal and conference articles.

Dr. Luo received the 2006 National Scientific and Technological Awards of China, the 2005 Scientific and Technological Awards from the National Mechanical Industry Association of China, and the 2007 Scientific and Technological Awards from the Hunan Province of China. He currently serves as the Associate Board Chairperson for the Hunan Society of Electrical Engineering. He also serves as the Chief of Hunan Electric Science and Application Laboratory.